Indian Journal of Pure & Applied Physics
Vol. 60, May 2022, pp. 437-448

Influences of Cattaneo-Christov Heat Flux, Joule Heating, Viscous Dissipation and Chemical Reaction on Hydromagnetic Pulsating Flow of Oldroyd-B Nanofluid in a Porous Channel

G Venkatesan & A Subramanyam Reddy*

Department of Mathematics, School of Advanced Sciences, Vellore Institute of Technology, Vellore, Tamil Nadu 632 014, India

Received 28 October 2021; accepted 19 April 2022

In this present study, Cattaneo-Christov heat flux on the hydromagnetic pulsatile flow of Oldroyd-B nanofluid through a porous channel with the presence of Brownian motion, thermal radiation, and thermophoresis effects are studied. The effects of dissipation of viscous and Ohmic heating are considered. The Buongiorno model is taken into account in this analysis. By using the perturbation method the governing partial differential equations (PDEs) are converted into the ordinary differential equations (ODEs) and solved numerically by employing the Runge-Kutta 4th-order scheme along with shooting approach. The influence of distinct parameters on velocity, temperature, nanoparticle concentration, heat and mass transfer rates are examined in detail. The results indicate that nanofluid velocity increases with higher frequency parameter, and while it falls with rising Hartmann number, and cross-flow Reynolds number. An increase in thermophoresis parameter, Eckert number, radiation parameter, Brownian motion parameter leads to a rise in temperature whereas temperature decreases for increasing Hartmann number and thermal relaxation time parameter. Moreover, the nanoparticle concentration enhances with an increasing thermophoresis parameter, thermal relaxation time parameter while it falls with the rising values of Lewis number, chemical reaction parameter and Brownian motion parameter.

Keywords: Pulsatile flow; Oldroyd-B nanoliquid; Cattaneo-Christov heat flux; Joule heating; chemical reaction; Brownian motion; thermophoresis

1 Introduction

The study of pulsatile flow has gotten a lot of attention of researchers because of its implementations in engineering and science, such as the reciprocal pumps, respiratory system, microelectromechanical system, vascular diseases, IC engines, and circulatory system[1-7]. Srinivas *et al.*[8] deliberated the influence of thermal diffusion, thermal radiation, and chemical reaction on the hydromagnetic pulsatile flow of non-Newtonian fluid in a channel. The governing flow equations were solved analytically by using the perturbation technique. Bilgi and Atalik[9] numerically explored the elastic properties of blood in terms of their effects on pulsatile arterial hemodynamics, such as the vorticity, velocity, stress fields, and indicators of aneurysm rupture. Ponalagusamy and Manchi[10] discussed the combined effects of magnetic and electrical fields on the pulsating flow of Jeffery fluid with particles suspended in stenosed arteries. Kumar and Srinivas[11] researched the pulsating flow of MHD blood-Al_2O_3/Cu/Ag/Au nanofluid in a vertical porous channel with velocity slip and Joule's heating impacts at the walls. Recently, Venkatesan and Reddy[12] analytically explored the hydromagnetic pulsatile flow of Au/CuO-blood non-Newtonian nanoliquid through a porous channel with Joule heating, dissipation of viscous, applied magnetic field, and thermal radiation effects.

The term nanofluid generally refers to the suspension of rigid nanometer-sized (1-100 nm) particles in a liquid. Choi[13] first proposed the development of nanofluid in 1995. Nanofluid is critically important in the modern world because of its wide array of applications in biomedicine, energy storage, cancer therapy, industrial cooling, nano-drug delivery, and electromechanical system[14-21]. Buongiorno[22] inspected the convective heat transfer in a nanoliquid. A two-component, non-homogeneous 4-equation equilibrium model for nanoliquid was developed by the author. Xu *et al.*[23] derived a mathematical model for the Buongiorno mixed convection flow of a nanofluid in a vertical channel by using the homotopy analysis method (HAM). Zheng *et al.*[24] studied the radiation heat transfer of a

*Corresponding author:
(E-mail: anala.subramanyamreddy@gmail.com)

nanofluid over a stretching sheet by using local similarity method. Srinivas *et al.*[25] intended the hydromagnetic flow of a nanoliquid through a porous channel along with slowly growing or shrinking walls by utilizing HAM. Kumar *et al.*[26] used the Buongiorno nanofluid model to analyse the hydromagnetic pulsating flow of non-Newtonian nanoliquid in a vertical channel inserted in a porous medium along with the presence of heat absorption and thermal radiation. Abdelmalek *et al.*[27] numerically examined impacts of thermophoretic diffusion and Brownian motion on electrically conducting nanofluid by employing R-K-Fehlberg method. Xu *et al.*[28] theoretically deliberated the applications of activation energy, induced magnetic force, and non-uniform heat sink/source on third grade nanofluid. Recently, Rajamani and Reddy[29] analytically studied the MHD pulsating flow of blood-Al_2O_3 non-Newtonian nanofluid through a channel based on the viscous dissipation and Ohmic heating effects by applying the perturbation method.

Many substances, such as lubricants, blood, ketchup, paints, dyes, ice creams, toothpaste, vaccines, cosmetics, syrups, and specific care products are non-Newtonian fluid, these do not obey the Newtonian manner. The non-Newtonian fluid model has been received much interest of several researchers[30-36]. Oldroyd-B fluid model is one of viscoelastic non-Newtonian fluid model. Malathy *et al.*[37] analytically explored the MHD pulsatile flow of an Oldroyd-B fluid with chemical reaction and radiation effects in a porous medium with convective and slip boundary conditions. Kumaran and Sandeep[38] theoretically inspected MHD non-Newtonian fluids towards a high revolutionary paraboloid with Brownian moment and numerically solved the governing equation by utilizing Runge-Kutta 4th-order scheme along with shooting technique. Javid *et al.*[39] evaluated the viscosity characteristics of non-Newtonian fluid with synthesized Fe_3O_4 added to glycerine, engine oil, paraffin oil, and distilled water for application in thermal system. Khan *et al.*[40] numerically researched the 2D steady non-Newtonian fluid flow and the heat transfer around a heated square cavity with a Y-shaped fin under the effects of thermal radiation and magnetic field by employing the Galerkin weighted residual technique of the finite element method. Recently, Venkatesan and Reddy[41] inspected the effects of the pulsating flow of blood-alumina Oldroyd-B (non-Newtonian) nanoliquid in a channel with Ohmic heating, dissipation of viscous, and magnetic field impacts by utilizing the perturbation method.

Heat transfer has a wide range of uses in current technology, including cooling nuclear reactors, magnetic drug targeting, medicinal application, and cooling of energy-producing areas, among others. The fundamental Fourier[42] law is one of the most well-known laws in classical physics for explaining the heat transfer process in a variety of situations. One of the fundamental flaws of the parabolic equation for heat is that is it causes disruption while also challenging the concept of determinism over the entire medium. Cattaneo[43] broke over this barrier by interlacing relaxation time with heat flux. Cattaneo's proposed model was improved by Christov[44], who included Oldroyd's upper convected derivatives. His adaptation is known as the Cattaneo-Christov heat flux model. Haddad[45] studied thermal instability in a Brinkman porous media with fluid inertia. There is research into both fixed-fixed and free-free boundaries. The Cattaneo-Christov theory has been incorporated into the constitutive heat flux equation. Ibrahim *et al.*[46] examined the impacts of Cattaneo-Christov heat and mass diffusions on viscoelastic nanofluid with 3rd order slip flow condition. Shah *et al.*[47] discussed non-isothermal micropolar fluid flow over a nonlinearly extending surface using Cattaneo-Christov heat flux model. Chu *et al.*[48] investigated the thermal and solutal relaxation characteristics of the prediction methodology of Cattaneo-Christov double diffusions on 2D magnetohydrodynamics boundary layer flow of second-grade nanofluid.

The survey bespeak that no attempt has yet been made to inspect Cattaneo-Christov heat flux model on the pulsating flow of Oldroyd-B nanoliquid through a porous channel with Brownian motion, chemical reaction, thermophoresis, Joule heating, and viscous dissipation effects. Based on previous studies, we made an attempt to examine the effects of chemical reactions, thermophoresis, Brownian motion, viscous dissipation, and Joule heating with Cattaneo-Christov heat flux model on the pulsatile hydromagnetic flow of Oldroyd-B within a porous channel. By using the perturbation method, the governing PDEs are reduced to ODEs and then numerically resolved by employing Runge-Kutta 4th-order scheme along with shooting method. The velocity, temperature, and nanoparticle concentration of nanofluid are discussed in detail with using pictorial results by varying various emerging parameters. The heat transfer rate and mass transfer

rate are deliberate using tables in detail for various parameters.

2 Formulation of the problem

Consider the incompressible and laminar hydromagnetic pulsating flow of Oldroyd-B nanofluid in a porous channel in the presence of Cattaneo-Christov heat flux. Joule heating, viscous dissipation, chemical reaction implication are taken into account. The Brownian motion and thermophoresis effects are analysing by using the Buongiorno nanofluid model. As shown in Fig. 1 Cartesian coordinate system is taken such that the x^*-axis is along to the bottom wall, and the y^*-axis is perpendicular to the walls. Fluid injected with velocity v_0 through the bottom wall and suctioned out through the top wall at the same rate. The walls are separated by the distance h. A strength of the magnetic field B_0 is consistently applied orthogonally to the walls. T_0 and C_0 are the temperature and nanoparticle concentration of bottom walls respectively. $T_1 (> T_0)$ and $C_1 (> C_0)$ are the temperature and nanoparticle concentration of top walls respectively. Assume that the pulsating flow is driven by an unsteady pressure gradient of the form [2, 3, 9, 26]

$$-\frac{1}{\rho_f}\frac{\partial P^*}{\partial x^*} = A(1+\varepsilon e^{i\omega t^*}), \qquad \ldots (1)$$

where ω is frequency, $\varepsilon (<<1)$ is a positive quantity, A is a constant, t^* is dimensional time, ρ_f is the density of the fluid. The current examination is constructed from the Oldroyd-B model on the viscoelastic fluid model. According to the aforementioned assumptions, the governing flow equations are

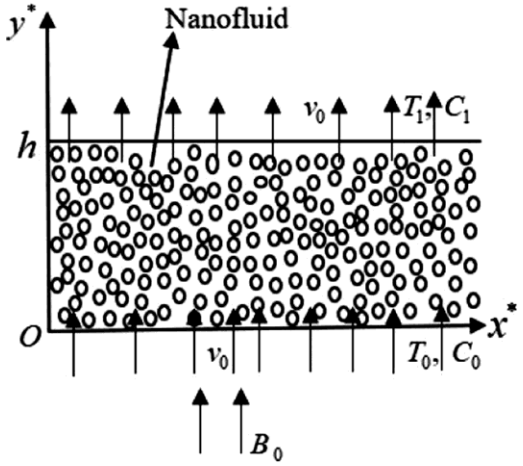

Fig. 1 — Flow geometry.

$$\left(1+\lambda_1\frac{\partial}{\partial t^*}\right)\frac{\partial u^*}{\partial t^*} + v_0\left(1+\lambda_1\frac{\partial}{\partial t^*}\right)\frac{\partial u^*}{\partial y^*} = -\frac{1}{\rho_f}\left(1+\lambda_1\frac{\partial}{\partial t^*}\right)\frac{\partial P^*}{\partial x^*} + \frac{\mu_f}{\rho_f}\left(1+\lambda_2\frac{\partial}{\partial t^*}\right)\frac{\partial^2 u^*}{\partial y^{*2}} - \frac{\sigma_f}{\rho_f}\left(1+\lambda_1\frac{\partial}{\partial t^*}\right)B_0^2 u^*, \qquad \ldots (2)$$

$$\frac{\partial T^*}{\partial t^*} + v_0\frac{\partial T^*}{\partial y^*} + \lambda_3\left(\frac{\partial^2 T^*}{\partial t^{*2}} + v_0^2\frac{\partial^2 T^*}{\partial y^{*2}} + 2v_0\frac{\partial^2 T^*}{\partial y^*\partial t^*}\right) = \frac{k_f}{(\rho C_p)_f}\frac{\partial^2 T^*}{\partial y^{*2}} - \frac{1}{(\rho C_p)_f}\frac{\partial q_r}{\partial y^*} + \frac{\mu_f}{(\rho C_p)_f}\left(\frac{\partial u^*}{\partial y^*}\right)^2 + \frac{\sigma_f}{(\rho C_p)_f}B_0^2 u^{*2} + \tau_1\left[D_B\left(\frac{\partial T^*}{\partial y^*}\frac{\partial C^*}{\partial y^*}\right) + \frac{D_T}{T_m}\left(\frac{\partial T^*}{\partial y^*}\right)^2\right], \qquad \ldots (3)$$

$$\frac{\partial C^*}{\partial t^*} + v_0\frac{\partial C^*}{\partial y^*} = D_B\frac{\partial^2 C^*}{\partial y^{*2}} + \frac{D_T}{T_m}\frac{\partial^2 T^*}{\partial y^{*2}} - k_r C^*, \qquad \ldots (4)$$

here, u^* is the dimensional velocity on x^* direction, T^* and C^* are the dimensional temperature and dimensional concentration of the fluid, P^* is the pressure, ν_f is the kinematic viscosity of the fluid, σ_f is the electrical conductivity of the fluid, λ_1 and λ_2 are relaxation and retardation times respectively, k_f is the thermal conductivity of the fluid, μ_f is the dynamic viscosity of the fluid, $(\rho C_P)_f$ is the effective heat capacity of fluid, λ_3 is the relaxation time of heat flux, D_B is Brownian diffusion coefficient, D_T is the thermophoretic diffusion coefficient, T_m is mean temperature, $\tau_1 = (\rho C_P)_p / (\rho C_P)_f$, $(\rho C_P)_p$ is the effective heat capacity of the nanoparticles and k_r is the first-order chemical reaction rate.

The corresponding boundary conditions (B.Cs) are as follows:

$$u^*(0)=0,\ T^*(0)=T_0,\ C^*(0)=C_0, \quad \ldots (5)$$

$$u^*(h)=0,\ T^*(h)=T_1,\ C^*(h)=C_1. \quad \ldots (6)$$

Now, with the use of Rosseland approximation for radiative heat flux, q_r and by following [24, 37] Eqn. (3) becomes

$$\frac{\partial T^*}{\partial t^*}+v_0\frac{\partial T^*}{\partial y^*}+\lambda_3\left(\frac{\partial^2 T^*}{\partial t^{*2}}+v_0^2\frac{\partial^2 T^*}{\partial y^{*2}}+2v_0\frac{\partial^2 T^*}{\partial y^*\partial t^*}\right)=\frac{k_f}{\left(\rho C_p\right)_f}\frac{\partial^2 T^*}{\partial y^{*2}}+\frac{\mu_f}{\left(\rho C_p\right)_f}\left(\frac{\partial u^*}{\partial y^*}\right)^2+\frac{\sigma_f}{\left(\rho C_p\right)_f}B_0^2u^{*2}+\frac{1}{\left(\rho C_p\right)_f}\frac{16T_1^3\hat{\sigma}}{3\xi}\frac{\partial^2 T^*}{\partial y^{*2}}+\tau_1\left[D_B\left(\frac{\partial T^*}{\partial y^*}\frac{\partial C^*}{\partial y^*}\right)+\frac{D_T}{T_m}\left(\frac{\partial T^*}{\partial y^*}\right)^2\right], \quad \ldots (7)$$

here, ξ is the Rosseland mean absorption co-efficient and $\hat{\sigma}$ is the Stefan-Boltzmann constant.

Now, by using the following non-dimensional parameters and variables,

$$\left.\begin{aligned} &x=\frac{x^*}{h},\ y=\frac{y^*}{h},\ P=\frac{P^*}{\rho_f Ah},\ u=\frac{\omega u^*}{A},\\ &t=t^*\omega,\ \theta=\frac{T^*-T_0}{T_1-T_0},\ \phi=\frac{C^*-C_0}{C_1-C_0}\end{aligned}\right\} \quad \ldots (8)$$

Eqns. (1), (2), (7), and (4) become

$$-\frac{\partial P}{\partial x}=1+\varepsilon e^{it}. \quad \ldots (9)$$

$$H^2\left(1+\lambda_1\omega\frac{\partial}{\partial t}\right)\frac{\partial u}{\partial t}+R\left(1+\lambda_1\omega\frac{\partial}{\partial t}\right)\frac{\partial u}{\partial y}=-H^2\left(1+\lambda_1\omega\frac{\partial}{\partial t}\right)\frac{\partial P}{\partial x}+\left(1+\lambda_2\omega\frac{\partial}{\partial t}\right)\frac{\partial^2 u}{\partial y^2}-M^2\left(1+\lambda_1\omega\frac{\partial}{\partial t}\right)u, \quad \ldots (10)$$

$$H^2\frac{\partial\theta}{\partial t}+R\frac{\partial\theta}{\partial y}+\delta\left[H^2\frac{\partial^2\theta}{\partial t^2}+\frac{R^2}{H^2}\frac{\partial^2\theta}{\partial y^2}+2R\frac{\partial^2\theta}{\partial y\partial t}\right]=\frac{1}{\mathrm{Pr}}\left(1+\frac{4}{3}Rd\right)\frac{\partial^2\theta}{\partial y^2}+Ec\left(\frac{\partial u}{\partial y}\right)^2+EcM^2u^2+Nb\frac{\partial\theta}{\partial y}\frac{\partial\phi}{\partial y}+Nt\left(\frac{\partial\theta}{\partial y}\right)^2, \quad \ldots (11)$$

$$H^2\,\mathrm{Pr}\,Le\frac{\partial\phi}{\partial t}+R\,\mathrm{Pr}\,Le\frac{\partial\phi}{\partial y}=\frac{\partial^2\phi}{\partial y^2}+\frac{Nt}{Nb}\frac{\partial^2\theta}{\partial y^2}-\gamma Le\,\mathrm{Pr}\,\phi-K_1Le\,\mathrm{Pr}, \quad \ldots (12)$$

where, $H=h\sqrt{\frac{\omega}{\nu_f}}$ is frequency parameter, $R=\frac{v_0h}{\nu_f}$ is cross-flow Reynolds number, $\alpha=\frac{k_f}{\left(\rho C_P\right)_f}$ is thermal diffusivity, $\delta=\omega\lambda_3$ is thermal relaxation time parameter, $M=B_0h\sqrt{\frac{\sigma_f}{\mu_f}}$ is Hartmann number, $Ec=\frac{A^2}{\omega^2\left(C_P\right)_f\left(T_1-T_0\right)}$ is Eckert number, $\mathrm{Pr}=\frac{\nu_f}{\alpha}$ is Prandtl number, $Rd=\frac{4\hat{\sigma}T_1^3}{k_f\zeta}$ is radiation parameter, $Nt=\frac{\tau_1D_T\left(T_1-T_0\right)}{T_m\nu_f}$ is thermophoresis parameter, $Nb=\frac{\tau_1D_B\left(C_1-C_0\right)}{\nu_f}$ is Brownian motion parameter, $\gamma=\frac{k_rh^2}{\nu_f}$ is chemical reaction parameter, $Le=\frac{\alpha}{D_B}$ is Lewis number and $K_1=\frac{k_rC_0h^2}{\nu_f\left(C_1-C_0\right)}$.

The corresponding B.Cs are

$$u(0)=0,\quad \theta(0)=0,\quad \phi(0)=0, \quad \ldots (13)$$

$$u(1)=0,\quad \theta(1)=1,\quad \phi(1)=1. \quad \ldots (14)$$

3 Method of Solution

In consideration of Eq. (9), we assume the dimensionless velocity u, temperature θ, and nanoparticle concentration ϕ are

$$\left.\begin{aligned} u(y)&=u_0(y)+\varepsilon e^{it}u_1(y),\\ \theta(y)&=\theta_0(y)+\varepsilon e^{it}\theta_1(y),\\ \phi(y)&=\phi_0(y)+\varepsilon e^{it}\phi_1(y)\end{aligned}\right\}. \quad \ldots (15)$$

Now, by substituting Eqns. (9) and (15) into (10)-(12) and equating the terms like various powers of ε, one can get

$$\frac{d^2u_0}{dy^2} - R\frac{du_0}{dy} - M^2u_0 + H^2 = 0, \quad \ldots (16)$$

$$\frac{d^2u_1}{dy^2} - R\beta^2\frac{du_1}{dy} - \left(M^2 + iH^2\right)\beta^2u_1 + \beta^2H^2 = 0, \quad \ldots (17)$$

$$\left(1 + \frac{4}{3}Rd - \delta\,\mathrm{Pr}\frac{R^2}{H^2}\right)\frac{d^2\theta_0}{dy^2} - R\,\mathrm{Pr}\frac{d\theta_0}{dy} + \mathrm{Pr}\,Nb\frac{d\theta_0}{dy}\frac{d\phi_0}{dy} + \mathrm{Pr}\,Nt\left(\frac{d\theta_0}{dy}\right)^2 + \mathrm{Pr}\,Ec\left(\frac{du_0}{dy}\right)^2 + \mathrm{Pr}\,EcM^2u_0^2 = 0, \quad \ldots(18)$$

$$\left(1 + \frac{4}{3}Rd - \delta\,\mathrm{Pr}\frac{R^2}{H^2}\right)\frac{d^2\theta_1}{dy^2} - i\,\mathrm{Pr}\,H^2\theta_1 - \mathrm{Pr}\,R\left(1 + 2i\delta\right)\frac{d\theta_1}{dy} + \mathrm{Pr}\,Nb\left(\frac{d\theta_0}{dy}\frac{d\phi_1}{dy} + \frac{d\theta_1}{dy}\frac{d\phi_0}{dy}\right) + 2\,\mathrm{Pr}\,Nt\frac{d\theta_0}{dy}\frac{d\theta_1}{dy} + 2\,\mathrm{Pr}\,Ec\frac{du_0}{dy}\frac{du_1}{dy} + 2\,\mathrm{Pr}\,EcM^2u_0u_1 + \delta\,\mathrm{Pr}\,H^2 = 0, \quad \ldots (19)$$

$$\frac{d^2\phi_0}{dy^2} - R\,\mathrm{Pr}\,Le\frac{d\phi_0}{dy} - \gamma Le\,\mathrm{Pr}\,\phi_0 + \frac{Nt}{Nb}\frac{d^2\theta_0}{dy^2} - K_1Le\,\mathrm{Pr} = 0, \quad \ldots (20)$$

$$\frac{d^2\phi_1}{dy^2} - R\,\mathrm{Pr}\,Le\frac{d\phi_1}{dy} - \left(\gamma + iH^2\right)Le\,\mathrm{Pr}\,\phi_1 + \frac{Nt}{Nb}\frac{d^2\theta_1}{dy^2} = 0, \quad \ldots (21)$$

where $\beta^2 = \dfrac{1 + \lambda_1 i\omega}{1 + \lambda_2 i\omega}$.

The corresponding B.Cs are

$$\left.\begin{aligned} &u_0(0) = 0, \quad \theta_0(0) = 0, \quad \phi_0(0) = 0, \\ &u_1(0) = 0, \quad \theta_1(0) = 0, \quad \phi_1(0) = 0 \end{aligned}\right\}, \quad \ldots (22)$$

$$\left.\begin{aligned} &u_0(1) = 0, \quad \theta_0(1) = 1, \quad \phi_0(1) = 1, \\ &u_1(1) = 0, \quad \theta_1(1) = 0, \quad \phi_1(1) = 0 \end{aligned}\right\}. \quad \ldots (23)$$

The physical quantities like heat and mass transfer rates (Nusselt and Sherwood numbers) in the dimensionless form at the walls are given as[2]

$$Nu = \left(\frac{d\theta_0}{dy} + \varepsilon\frac{d\theta_1}{dy}e^{it}\right)_{y=0,1}, \quad \ldots (24)$$

$$Sh = \left(\frac{d\phi_0}{dy} + \varepsilon\frac{d\phi_1}{dy}e^{it}\right)_{y=0,1}. \quad \ldots (25)$$

Now, The system of Eqns. (16)-(21) with the B.Cs (22)-(23) are solved numerically by utilizing Ruge-Kutta fourth-order scheme using the shooting method. The step size is fixed as 0.001 ($\Delta y = 0.001$). 1×10^{-10} correctness is fixed for the converging criteria.

To ensure the correctness of the current results, we compared them with the results obtained by NDSolve using the MATHEMATICA software, which are shown in Table 1. It can be seen that there is a good agreement between the results obtained by NDSolve and the current results.

Table 1 — Comparison between the present results and the results obtained by NDSolve for heat and mass transfer rates at the wall $y = 0$ for different values of M, and δ when $H = 2$, $R = 0$, $Ec = 0.5$, $\mathrm{Pr} = 21$, $Rd = 1$, $Nb = 0.2$, $Nt = 0.2$, $Le = 2$, $K_1 = 0.001$, $\gamma = 1$, $\lambda_1 = 0.5$, $\lambda_2 = 0.8$, $\omega = 2$, $t = \pi/3$, $\varepsilon = 0.001$.

Parameters	values	$\theta'(y)$ at $y=0$		$\phi'(y)$ at $y=0$	
		NDSolve	Present result	NDSolve	Present result
M	1	9.9790097	9.9790095	-5.751406	-5.751403
	2	9.0977212	9.0977186	-5.020325	-5.020321
	3	7.7060661	7.7060645	-3.990262	-3.990260
δ	0.1	9.0977212	9.0977186	-5.020325	-5.020321
	0.3	9.1012676	9.1012657	-5.022169	-5.022166
	0.5	9.1048140	9.1048120	-5.024014	-5.024010

4 Result and discussion

The existing sector describes the influence of different values of several parameters on velocity, temperature, and nanoparticle concentration distribution which are given in Figs. 2-7. In this present analysis u_s, θ_s, and ϕ_s are represent steady velocity, steady temperature, and steady nanoparticle concentration respectively. u_t, θ_t, and ϕ_t are represents unsteady velocity, unsteady temperature, and unsteady nanoparticle concentration of Oldroyd-B nanoliquid respectively. Throughout the analysis the parameters' values are taken as $H=2,\ M=2,\ R=1,\ Ec=0.5,\ \Pr=21,\ Rd=1,\ Nb=0.2,$ $Nt=0.2,\ Le=2,\ K_1=0.001,\ \gamma=1,\ \lambda_1=0.5,$ $\lambda_2=0.8,\ \delta=0.1,\ \omega=2,\ t=\pi/3,\ \varepsilon=0.001$, unless otherwise stated. The steady velocity distribution of Oldroyd-B nanofluid for various values of frequency parameter (H), Hartmann number (M), and cross-flow Reynolds number (R) are illustrated in Figs. 2(a-c). Fig. 2(a) indicates that greater frequency parameter increases the steady velocity u_s. The reason is that an increase in frequency rises the velocity of the nanofluid. The steady velocity declines with increasing Hartmann number, as shown in Fig. 2(b). The purpose for the decrease in velocity is that the retarding forces which are created by the applied magnetic field are acted orthogonal to the flow direction and hence there is a decrease in the velocity. Fig. 2(c) shows that increasing R expedites steady velocity near the top wall while it retards near the bottom wall. The unsteady velocity distribution of Oldroyd-B nanofluid for various values of frequency parameter (H), Hartmann number (M), non-Newtonian parameters (λ_1,λ_2), cross-flow Reynolds number (R), and time (t) are shown in Figs. 3(a-f). Fig. 3(a) describes the growth in H rises the unsteady velocity because a rise in frequency boosts up the velocity of the nanofluid. Fig. 3(b) illustrates increasing M causes decline in unsteady velocity. This decline is by reason of Lorentz's force generated by the applied magnetic field inside the system. The unsteady velocity is an increasing function of λ_1 (see Fig. 3(c)). The opposite behavior is portrayed in Fig. 3(d) by the various values of λ_2. Fig. 3(e) represents u_t accelerate closer to the suction wall (top wall) while it falling closer to the injection wall (bottom wall) for increasing R. From Fig. 3f one can notice that u_t is fluctuating for different values of t.

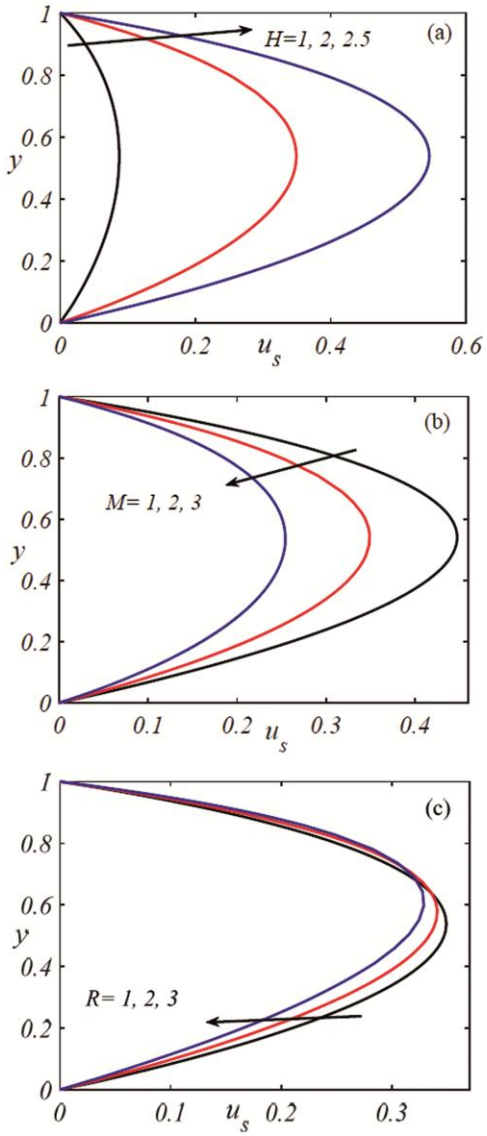

Fig. 2 — Steady velocity (a) influence of $H=1,2,2.5$, (b) influence of $M=1,2,3$, (c) influence of $R=1,2,3$

Figs. 4(a-f) illustrate the impacts of Eckert number (Ec), radiation parameter (Rd), thermal relaxation time parameter (δ), Hartmann number (M), Brownian motion parameter (Nb), and thermophoresis parameter (Nt) respectively on steady temperature θ_s of nanoliquid. As seen in Fig. 4(a), increasing Ec rises the steady temperature of nanofluid. Ec is the relationship between the enthalpy and the kinetic energy. An increases in Ec leads to boost up the kinetic energy of particles by reducing enthalpy factor and that rises the temperature of the nanofluid.

he effect of Rd on θ_s is presented in Fig. 4(b). It shows that larger Rd generates extra heat within the system, which will enhance thermal boundary layers. Therefore, rising Rd increases θ_s of the nanofluid. From Fig. 4(c) one can depicts that rising δ reduces the fluid temperature. The reason is that for higher values of thermal relaxation parameter δ the particles of quantifiable material have a greater chance of supplying heat to their adjacent particles when the relaxation time parameter of heat flux is increased, thus the temperature reduces. According to Fig. 4(d), a higher Hartmann number declines the steady temperature of nanofluid. There is a possibility that Lorentz's force generated by an applied magnetic field converts to a resistive drag force, which would explain this decline. Fig. 4(e) portrays the influence of Nb on θ_s. It is clear that rising Nb substantially boosts the fluid temperature. The same nature, we can be seen in Fig. 4(f) by varying Nt.

The effects of M, Ec, λ_1, λ_2, Rd and δ on θ_t are demonstrated in Figs. 5(a-f) respectively. From these figures one can see that θ_t is wavering and the

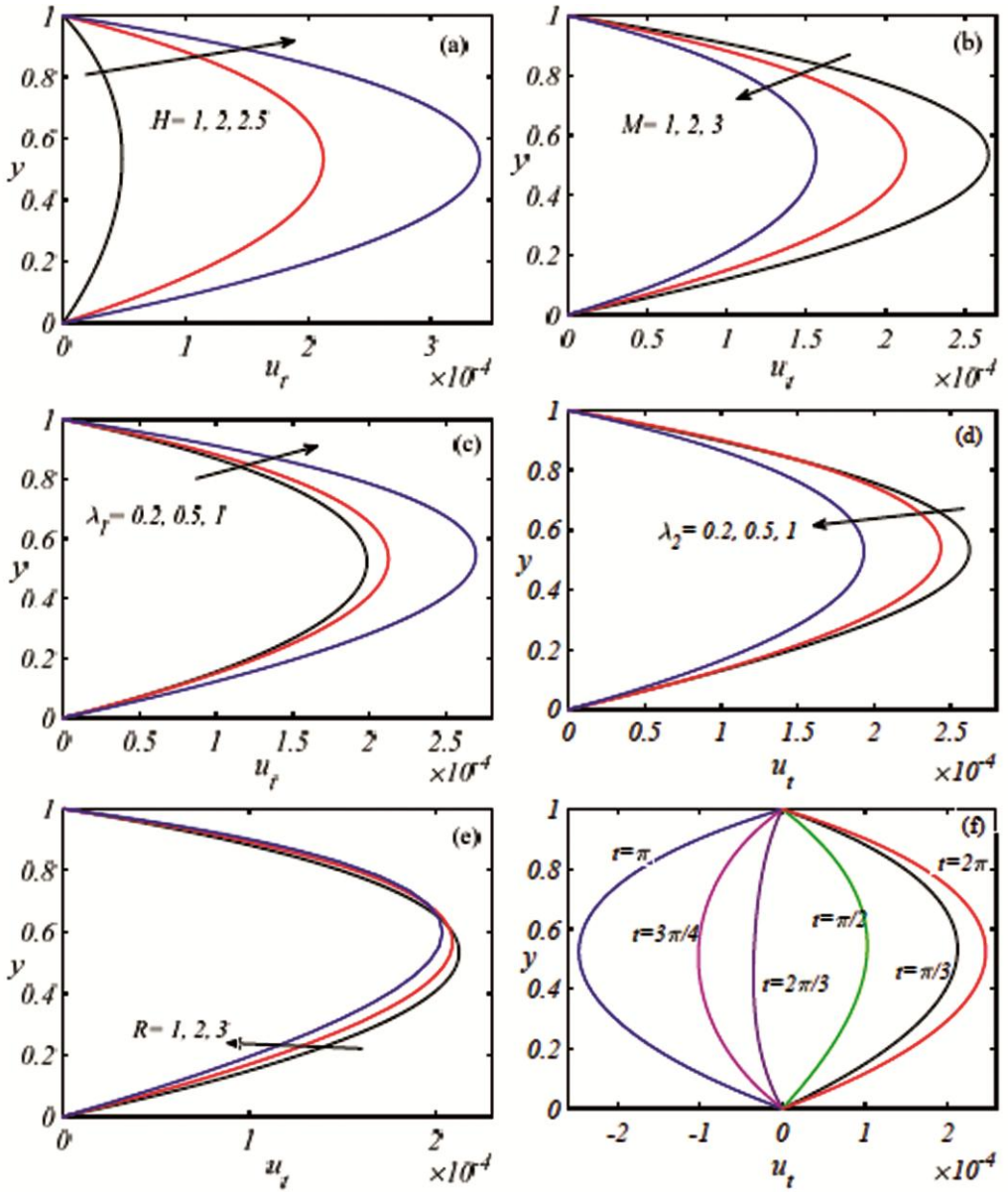

Fig. 3 — Unsteady velocity (a) influence of $H = 1, 2, 2.5$, (b) influence of $M = 1, 2, 3$, (c) influence of $\lambda_1 = 0.2, 0.5, 1$, (d) influence of $\lambda_2 = 0.2, 0.5, 1$, (e) influence of $R = 1, 2, 3$, and (f) influence of $t = \pi, \frac{3\pi}{4}, \frac{2\pi}{3}, \frac{\pi}{2}, \frac{\pi}{3}, 2\pi$

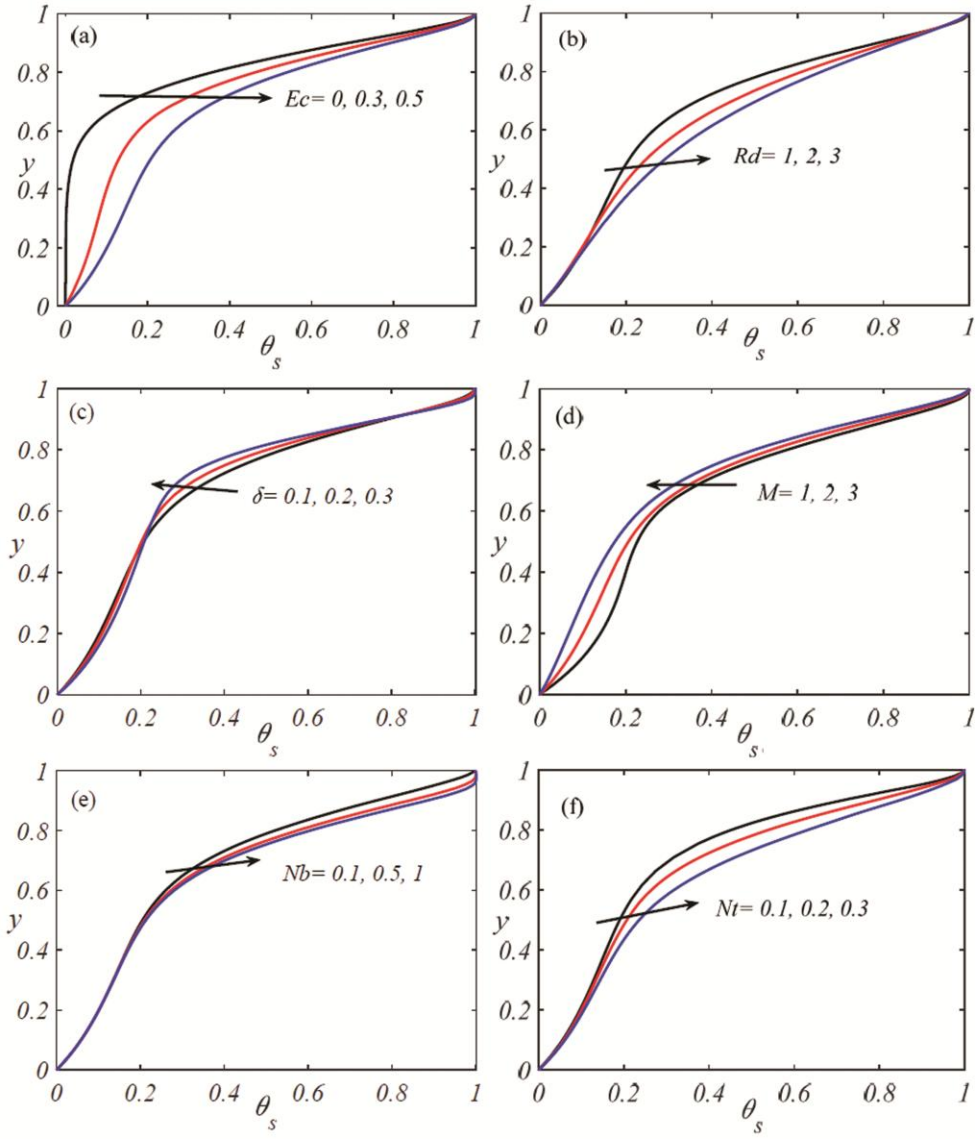

Fig. 4 — Steady temperature (a) influence of $Ec = 0, 0.3, 0.5$, (b) influence of $Rd = 1, 2, 3$, (c) influence of $\delta = 0.1, 0.2, 0.3$, (d) influence of $M = 1, 2, 3$, (e) influence of $Nb = 0.1, 0.5, 1$, (f) influence of $Nt = 0.1, 0.2, 0.3$

utmost is near the suction wall. Fig. 5(a) shows that escalating M wavering θ_t. Fig. 5(b) displays that up rise Ec escalates θ_t. The reason is that the heat generated by viscous dissipation may be responsible for this temperature escalates. The same action can be noted that in Fig. 5(c) by growing λ_1. θ_t is a decreasing function of λ_2 (see Fig. 5(d)). Fig. 5(e) shows that θ_t is oscillating for higher Rd. Fig. 5(f), detected that θ_t rises for increasing δ.

Figures. 6(a-e) demonstrate the impacts of chemical reaction (γ), Lewis number (Le), thermophoresis parameter (Nt), Brownian motion parameter (Nb), and thermal relaxation time parameter (δ) on nanoparticle concentration of nanofluid correspondingly. Fig. 6(a) discloses that ϕ_s is reduced for a given rise in the chemical reaction parameter γ. The effect of Le on ϕ_s is portrayed in Fig. 6(b). As one might expect that increasing Lewis number reduces ϕ_s. This may be because an increase in Lewis number increases the rate of mass transfer and thus reduces the nanoparticles concentration. Fig. 6(c) reveals that ϕ_s improves for a better estimate of Nt. The steady nanoparticle concentration

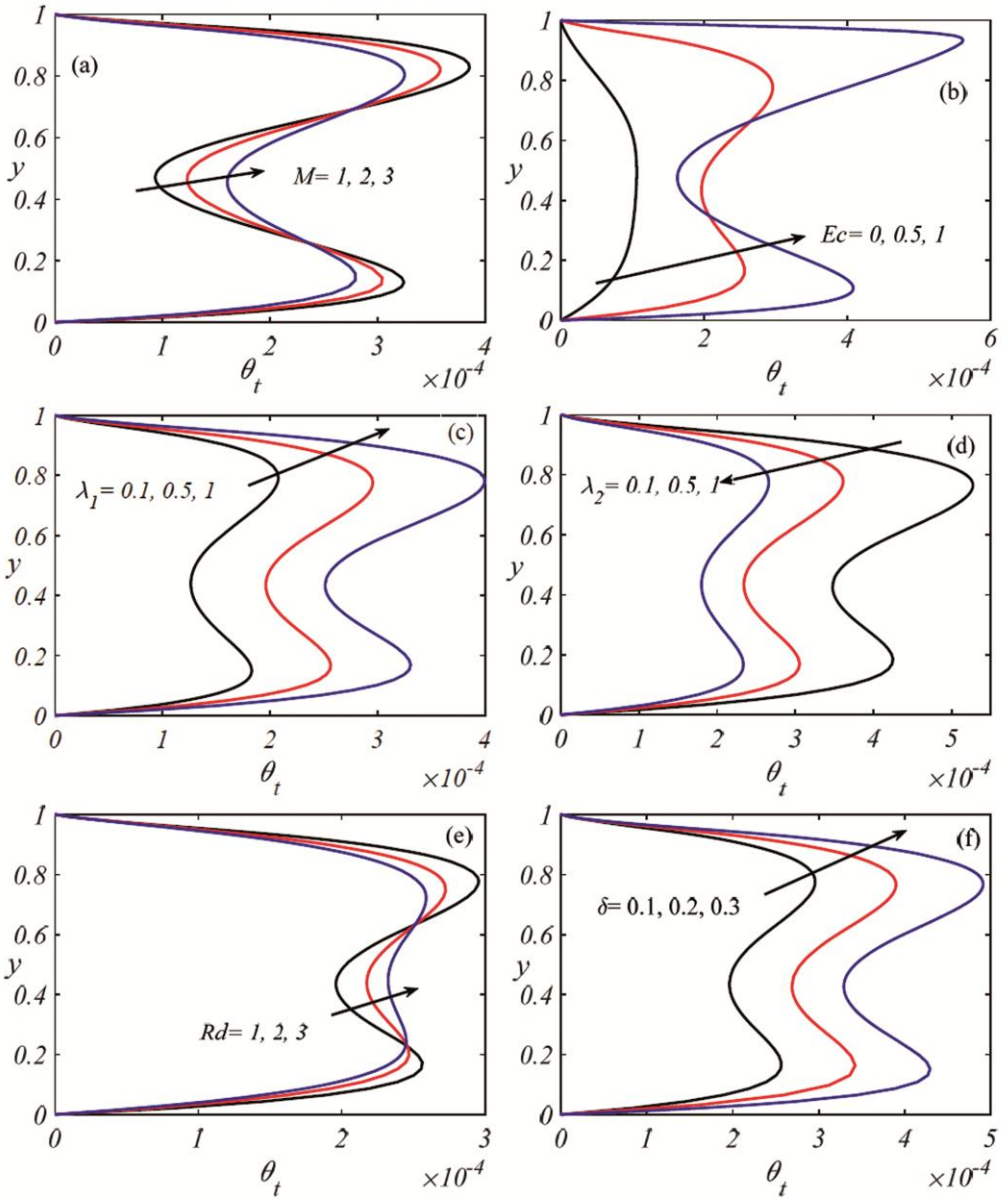

Fig. 5 — Unsteady temperature when $H = 2.5$ (a) influence of $M = 1, 2, 3$, (b) influence of $Ec = 0,\ 0.5, 1$, (c) influence of $\lambda_1 = 0.2, 0.5, 1$, (d) influence of $\lambda_2 = 0.2, 0.5, 1$, (e) influence of $Rd = 1, 2, 3$ and (f) influence of $\delta = 0.1, 0.2, 0.3$

decreases as Nb increases because nanoparticles collide more rapidly and more heat is produced (see Fig. 6(d)). The contrary action can be seen in Fig. 6(e) for higher δ.

Figures. 7(a-d) contrived the inspirations of Nb, Nt, δ and t on ϕ_t. Fig. 7(a) depicts that increasing Nb enhanced ϕ_t near the walls while it falls near the middle of the channel. The opposite behavior is depicted in Figs. 7(b) & (c) by varying Nt and δ respectively. Fig. 7(d) shows that ϕ_t is oscillating nature for different values of t, and maximum near the top wall. Also, we can see that in these figures, ϕ_t is wavering nature.

Table 2 shows the variations in the steady heat transfer rate (steady Nusselt number (Nu_s)), unsteady heat transfer rate (unsteady Nusselt number (Nu_t)), the steady mass transfer rate (steady Sherwood number (Sh_s)), and unsteady mass transfer rate (unsteady

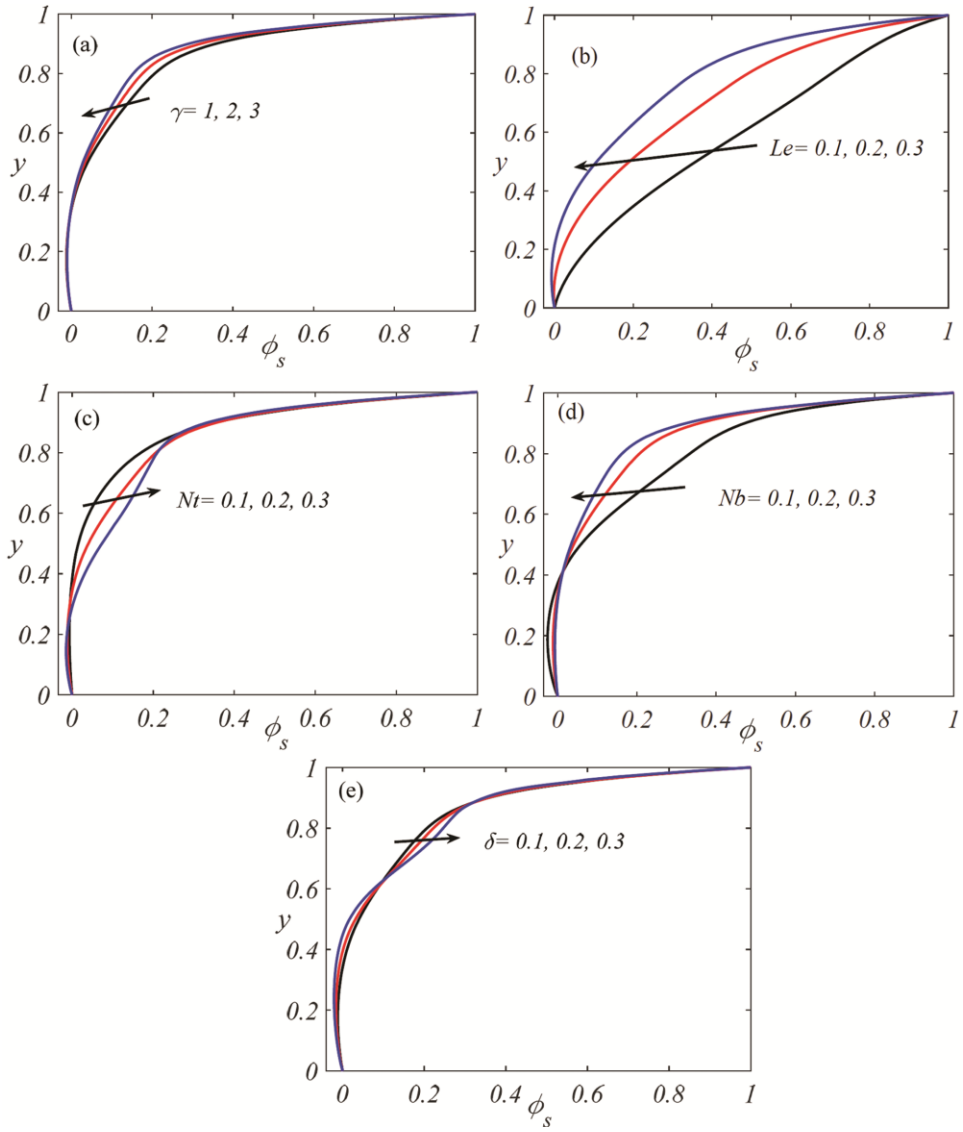

Fig. 6 — Steady nanoparticle concentration when $Le = 0.5$ (a) influence of $\gamma = 1, 2, 3$, (b) influence of $Le = 0.1, 0.2, 0.3$, (c) influence of $Nt = 0.1, 0.2, 0.3$, (d) influence of $Nb = 0.1, 0.2, 0.3$ and (e) influence of $\delta = 0.1, 0.2, 0.3$

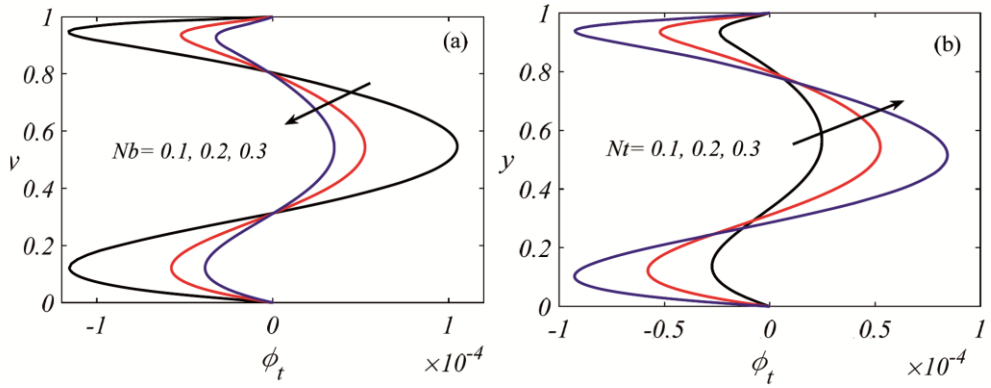

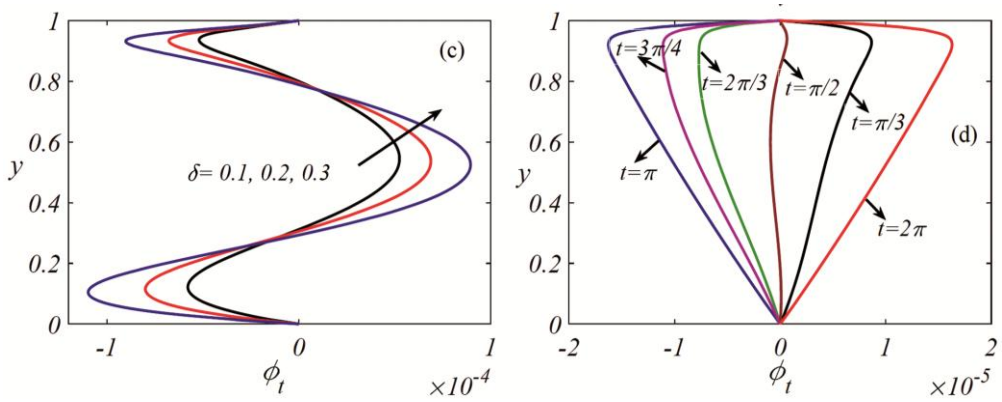

Fig. 7 — Unsteady nanoparticle concentration when $H = 2.5$ (a) influence of $Nb = 0.1, 0.2, 0.3$, (b) influence of $Nt = 0.1, 0.2, 0.3$, (c) influence of $\delta = 0.1, 0.2, 0.3$, and (d) influence of $t = \pi, \frac{3\pi}{4}, \frac{2\pi}{3}, \frac{\pi}{2}, \frac{\pi}{3}, 2\pi$

Table 2 — Variations of steady Nusselt number $Nu_s = \left(\theta_0'(y)\right)$, unsteady Nusselt number $Nu_t = \left(\varepsilon\theta_1'(y)e^{it}\right)$, steady Sherwood number $Sh_s = \left(\phi_0'(y)\right)$, and unsteady Sherwood number $Sh_t = \left(\varepsilon\phi_1'(y)e^{it}\right)$ at the wall $y = 0$ for various values of Ec, Nb, Nt, M, Rd, δ when $\Pr = 21$, $K_1 = 0.001$, $\gamma = 1$, $\lambda_1 = 0.5$, $\lambda_2 = 0.8$, $\omega = 2$, $t = \pi/3$, $\varepsilon = 0.001$

Parameter	values	Nu_s	Nu_t	Sh_s	Sh_t
Ec	0	0.000659	0.000627	-0.000733	-0.000059
	0.5	0.700450	0.002367	-0.058586	-0.000428
	1	1.557516	0.004565	-0.139153	-0.001016
Nb	0.1	0.700364	0.002362	-0.116278	-0.000855
	0.2	0.700450	0.002367	-0.058586	-0.000428
	0.3	0.700507	0.002371	-0.039361	-0.000285
Nt	0.1	0.669287	0.002191	-0.027867	-0.000183
	0.2	0.700450	0.002367	-0.058586	-0.000428
	0.3	0.739908	0.002594	-0.093907	-0.000758
M	1	1.050273	0.003087	-0.092007	-0.000635
	2	0.700450	0.002367	-0.058586	-0.000428
	3	0.436252	0.001789	-0.035218	-0.000277
Rd	1	0.700450	0.002367	-0.058586	-0.000428
	2	0.621620	0.001672	-0.041757	-0.000229
	3	0.613134	0.001354	-0.029413	-0.000157
δ	0.1	0.700450	0.002367	-0.058586	-0.000428
	0.2	0.761188	0.003822	-0.067040	-0.000786
	0.3	0.844957	0.006659	-0.078440	-0.001761

Sherwood number (Sh_t)) at the lower wall for various values of Ec, Nb, Nt, M, Rd, and δ. One can be noted that both Nu_s and Nu_t are increased with the rise in Eckert number (Ec), Brownian motion parameter (Nb), thermophoresis parameter (Nt), and thermal relaxation time parameter (δ). Furthermore, it is observed that Nu_s and Nu_t are decreasing functions of Hartmann number (M), and radiation parameter (Rd). This table exhibition Sh_s and Sh_t are decreased for a given rise Nt, Ec and δ. Furthermore, from this table one can note that Sh_s and Sh_t are increasing functions of M, Nb, and Rd.

5 Conclusion

This study examines the pulsatile flow of Oldroyd-B nanofluid in a porous channel subjected to a chemical reaction, viscous dissipation, and Joule heating with the Cattaneo-Christov heat flux model. By using the perturbation approach, the PDEs are converted into ODEs and solved numerically using the Runge-Kutta fourth-order scheme using the shooting approach. The effects of relevant parameters

have been analyzed on the flow variables. The most important results are as follows:

- The steady velocity increases with higher frequency parameter, and while it falls with rising Hartmann number, and cross-flow Reynolds number.
- The unsteady velocity of nanofluid enhances with a rise in λ_1, H while it is reduced with a rise in M, λ_2, R.
- There is an enhancement in θ_s of nanofluid for the higher values of Ec, Rd, Nb and Nt.
- θ_t distribution demonstrates wavering nature and the supreme is near the suction wall.
- The steady nanoparticle concentration distribution declines with a gain of Le, γ, Nb while it grows for a given rise in Nt and δ.
- Nu_s and Nu_t are increasing functions of Nb, Nt, Ec and δ.
- Sh_s and Sh_t are reducing functions of Nt, δ and Ec while they are increasing functions of Nb, M, and Rd.

References

1 Wang C Y, *J Appl Mech Trans ASME*, 38 (1971) 553.
2 Radhakrishnamacharya G & Maiti M K, *Int J Heat Mass Transfer*, 20 (1977) 171.
3 Datta N, Dalal D C & Mishra S K, *Int J Heat Mass Transfer*, 36 (1993) 1783.
4 Shawky H M, *Heat Mass Transfer*, 45 (2009) 1261.
5 Selimefendigil F & Oztop H F, *Int Commun Heat Mass Transfer*, 45 (2013) 111.
6 Pan J, Bian Y, Liu Y, Zhang F, Yang Y, & Arima H, *Inter J Heat Mass Transfer*, 147 (2020) 118932.
7 Bukhari Z, Ali A, Abbas Z & Farooq H, *AIP Advances*, 11 (2021) 1.
8 Srinivas S, Kumar C K, & Reddy A S, *Nonlinear Anal Model Control*, 23 (2018) 213.
9 Bilgi C & Atalik K, *J Non-Newtonian Fluid Mech*, 279 (2020) 104263.
10 Ponalagusamy R & Manchi R, *Eur J Mech, B/Fluids*, 81(2020) 76.
11 Kumar P B & Srinivas S, *Eur Phy J Spe Top*, 123, (2021).
12 Venkatesan G & Reddy A S, *Heat Transfer* 50 (2021) 7495.
13 Choi S U S, *FED - Am Soc Mech Eng Fluids Eng Div Newsl*, 231 (1995) 99.
14 Hatami M, Hatami J & Ganji D D, *Comput Meth Prog Biomed*, 113 (2014) 632.
15 Uddin M J, Bég O A, Aziz A & Ismail A I M, *Math Prob Eng*, (2015).
16 Raju C S K, Sandeep N & Kumaran G, *J Comput Appl Res Mech Eng*, 7 (2018) 209.
17 Rashad A M, Khan W A, Tlili I & EL-Hakiem A M A, *Indian J Pure Appl Phys*, 57 (2019) 773.
18 Sandhya A, Reddy G V R & Deekshitulu G V S R, *Indian J Pure Appl Phys*, 58 (2020) 548.
19 Chaudhary S & Chouhan K K, *Indian J Pure Appl Phys*, 59 (2021) 559.
20 Vijayaragavan R, Bharathi V & Prakash J, *Indian J Pure Appl Phys*, 59 (2021) 28.
21 Rajkumar D & Reddy A S, *Phys Scr*, (2021) https://doiorg/101088/1402-4896/ac2e81.
22 Buongiorno J, *J Heat Transfer*, 128 (2006) 240.
23 Xu H, Fan T & Pop I, *Int Commun Heat Mass Transfer*, 44 (2013) 15.
24 Zheng L, Zhang C, Zhang X & Zhang J, *J Franklin Inst*, 350 (2013) 990.
25 Srinivas S, Vijayalakshmi A, Ramamohan T R, & Reddy A S, *J Porous Med*, 17 (2014) 953.
26 Kumar C K, Srinivas S & Reddy A S, *J Mech*, 36 (2020) 535.
27 Abdelmalek Z, Hussain A, Bilal S, Sherif E S M & Thounthong P, *J Mater Res Tech*, 9 (2020) 11948.
28 Xu Y J, Khan S U, Al-Khaled K, Khan M I, Alzahrani F & Khan M I, *Case Stud Therm Eng*, 27 (2021) 101305.
29 Rajamani S & Reddy A S, *Proc Inst Mech Eng Part E: J Process Mech Eng*, 235 (2021) 1895.
30 Oldroyd J G, *Proc Royal Soc London Series A Math Phy Sci*, 200 (1950) 523.
31 Rajagopal K R & Bhatnagar R K, *Acta Mechanica*, 113 (1995) 233.
32 Fetecau C & Fetecau C, *Int J Non-Linear Mech*, 38 (2003) 1539.
33 Khan M, Saleem M, Fetecau C & Hayat T, *Int J Non-Linear Mech*, 42 (2007) 1224.
34 Hayat T, Javed T & Abbas Z, *Int J Heat Mass Transfer*, 51 (2008) 4528.
35 Khan M, Hayat T & Wang Y, *Acta Mechanica Sinica/Lixue Xuebao*, 24 (2008) 51.
36 Wang J, Khan M I, Khan W A, Abbas S Z & Khan M I, *Comput Methods Prog Biomed*, 189 (2020) 105310.
37 Malathy T, Srinivas S & Reddy A S, *J Porous Media*, 20 (2017) 287.
38 Kumaran G & Sandeep N, *J Mol Liq*, 233 (2017) 262.
39 Javid M A, Habib T & Nadeem K, *Mater Today Proc*, (2020).
40 Khan Z H, Khan W A & Hamid M, *J Therm Anal Calor*, 143 (2021) 573.
41 Venkatesan G & Reddy A S, *Eur Phy J Spe Top*, 230 (2021) 1475.
42 Fourier J B J, *Théorie analytique de la chaleur* Chez Firmin Didot, (1822).
43 Cattaneo C, *Atti Sem Mat Fis Univ Modena*, 3 (1948) 83.
44 Christov C I, *Mech Res Commun*, 36 (2009) 481.
45 Haddad S A M, *Int J Heat Mass Transfer*, 68 (2014) 659.
46 Ibrahim W, Dessale A & Gamachu D, *Propuls Power Res*, 10 (2021) 180.
47 Shah Z, Shutaywi M, Dawar A, Kumam P, Thounthong P & Islam S, *J Mater Res Tech*, 9 (2020) 5452.
48 Chu Y M, Shah F, Khan M I, Kadry S, Abdelmalek Z & Khan W A, *J Mater Res Tech*, 9 (2020) 13977.